A kernel extension of the Ensemble Transform Kalman Filter

Sophie Mauran[1][0000−0001−7176−2684],
Sandrine Mouysset[2][0000−0003−0407−0527],
Ehouarn Simon[1][0000−0003−3205−1649], and
Laurent Bertino[3][0000−0002−1220−7207]

[1] Université de Toulouse, INP, IRIT, 2 Rue Charles Camichel, Toulouse, France
[2] Université de Toulouse, UT3, IRIT, Cr Rose Dieng-Kuntz, Toulouse, France
[3] Nansen Environmental and Remote Sensing Center, Jahnebakken 3 N-5007, Bergen, Norway

Abstract. Data assimilation methods are mainly based on the Bayesian formulation of the estimation problem. For cost and feasibility reasons, this formulation is usually approximated by Gaussian assumptions on the distribution of model variables, observations and errors. However, when these assumptions are not valid, this can lead to non-convergence or instability of data assimilation methods. The work presented here introduces the use of kernel methods in data assimilation to model uncertainties in the data in a more flexible way than with Gaussian assumptions. The use of kernel functions allows to describe non-linear relationships between variables. The aim is to extend the assimilation methods to problems where they are currently unefficient. The Ensemble Transform Kalman Filter (ETKF) formulation of the assimilation problem is reformulated using kernels and show the equivalence of the two formulations for the linear kernel. Numerical results on the toy model *Lorenz 63* are provided for the linear and hyperbolic tangent kernels and compared to the results obtained by the ETKF showing the potential for improvement.

Keywords: data assimilation · kernel methods · ensemble Kalman filters.

1 Introduction

Data assimilation is a process that consists of estimating the state of a system from observations and a numerical model of this system. This field of research has many applications, for example in meteorology ([1], [2], [3]) or oceanography ([2], [4], [5]). The resolution on this type of large-scale systems involves a large number of state and observation variables, sometimes of the order of a billion ([4]). In view of the complexity of these systems, several simplifications in the resolution are made and in particular assumptions of Gaussianity of the uncertainties on the observations and on the predictions ([2]).

ICCS Camera Ready Version 2023
To cite this paper please use the final published version:
DOI: 10.1007/978-3-031-36027-5_35

However, these assumptions are often not satisfied in practice and it happens that the non-respect of these assumptions leads to problems in the assimilation process, either prediction errors or instabilities of the method ([6]). To overcome these different problems, several approaches have been put forward, such as Gaussian anamorphoses ([7], [8]) or 2-step Bayesian updates ([9]). In this paper, we investigate kernel methods. Recent works [10] proposed a first formulation of an ensemble-based data assimilation algorithm based on "RBF" (radial-basis-function) kernels; [11]). It is then proposed to approximate the innovation term by a linear combination of RBF kernels, which parameters are estimated during the assimilation process. The introduction of RKHS is also proposed to model the temporal evolution of the dynamical system in order to apply ensemble methods in data assimilation [12], [13]. Furthermore, the analysis step of the Random Feature Map Data Assimilation algorithm [[13]] can be viewed as the application of an ensemble Kalman filter in a particular RKHS. In this work, we are reformulating a data assimilation ensemble algorithm, the Ensemble Transform Kalman Filter, as an optimization problem on any RKHS, in order to extend the approach to a nonlinear framework, with limited loss of optimality. First, we reformulate the ETKF as presented in [14] using kernel methods and present a way to reconstruct the ensemble based on this formulation. We then give numerical results for the Lorenz 63 toy model for the linear kernel and the hyperbolic tangent kernel.

2 ETKF reformulation with kernel methods

In this section, we first present the classical ETKF formulation and its resolution and then we present the corresponding kernel version.

2.1 ETKF formulation and classical resolution

The ETKF (Ensemble Transform Kalman Filter) problem is a classical formulation of the data assimilation problem, proposed by [14]. Its formulation derives from:

$$\arg\min_{\mathbf{w}\in\mathbb{R}^N} \mathcal{J}(\mathbf{w}) = \frac{N-1}{2}||\mathbf{w}||_2^2 + \frac{1}{2}||\mathbf{y} - \mathcal{H}(\bar{\mathbf{x}}^\mathbf{f} + \mathbf{X}^\mathbf{f}\mathbf{w})||^2_{\mathbf{R}^{-1}} \tag{1}$$

where $\bar{\mathbf{x}}^\mathbf{f} \in \mathbb{R}^n$ the ensemble mean obtained after the prediction step, $\mathbf{X}^\mathbf{f} = \left[(\mathbf{x}_\mathbf{1}^\mathbf{f} - \bar{\mathbf{x}}^\mathbf{f}), \ldots, (\mathbf{x}_\mathbf{N}^\mathbf{f} - \bar{\mathbf{x}}^\mathbf{f})\right] \in \mathbb{R}^{n\times N}$ the ensemble anomaly matrix obtained after the prediction step, $\mathcal{H} : \mathbb{R}^n \to \mathbb{R}^p$ the transition operator between the model space and the observation space, $\mathbf{w}$ parameterizing $\mathbf{x}^\mathbf{a}$: $\mathbf{x}^\mathbf{a} = \bar{\mathbf{x}}^\mathbf{f} + \mathbf{X}^\mathbf{f}\mathbf{w}$, under the assumption that $\mathbf{x}^\mathbf{a}$ lies in the affine subspace of $\bar{\mathbf{x}}^\mathbf{f}$ generated by $\mathbf{X}^\mathbf{f}$, N the ensemble size, $\mathbf{y} \in \mathbb{R}^p$ the observation vector, $\mathbf{R} \in \mathbb{R}^{p\times p}$ the error covariance matrix of the observations and $||.||_{\mathbf{R}^{-1}}$ defined by $||\mathbf{x}||^2_{\mathbf{R}^{-1}} = \mathbf{x}^\top\mathbf{R}^{-1}\mathbf{x}$

For the sake of simplicity, we assume that the observation operator $\mathcal{H}$ is linear. We can then rewrite (1) as:

ICCS Camera Ready Version 2023
To cite this paper please use the final published version:
DOI: 10.1007/978-3-031-36027-5_35

$$\underset{\mathbf{w}\in\mathbb{R}^N}{\arg\min}\,\mathcal{J}(\mathbf{w}) = \frac{N-1}{2}||\mathbf{w}||_2^2 + \frac{1}{2}||\mathbf{y} - \mathbf{H}\bar{\mathbf{x}}^{\mathbf{f}} - \mathbf{H}\mathbf{X}^{\mathbf{f}}\mathbf{w}||_{\mathbf{R}^{-1}}^2 \tag{2}$$

with $\mathbf{H}$ the observation operator.

Here, for the sake of later clarity, we introduce some additional notations: $\widetilde{\mathbf{d}} = \mathbf{R}^{-1/2}(\mathbf{y} - \mathbf{H}\bar{\mathbf{x}}^{\mathbf{f}}) \in \mathbb{R}^p$ and $\widetilde{\mathbf{H}} = \mathbf{R}^{-1/2}\mathbf{H}\mathbf{X}^{\mathbf{f}} = \begin{bmatrix} \widetilde{\mathbf{h_1}}^\top \\ \vdots \\ \widetilde{\mathbf{h_p}}^\top \end{bmatrix} \in \mathbb{R}^{p\times N}$.

The first order optimality condition yields $\mathbf{w}^*$ solution of (2):

$$\mathbf{w}^* = [(N-1)\mathbf{I} + \widetilde{\mathbf{H}}^\top\widetilde{\mathbf{H}}]^{-1}\widetilde{\mathbf{H}}^\top\widetilde{\mathbf{d}} \tag{3}$$

We then generate the ensemble members noted $\mathbf{x_i^a} \in \mathbb{R}^n$, $\forall\, i \in \{1, ..., N\}$:

$$\mathbf{x_i^a} = \bar{\mathbf{x}}^{\mathbf{f}} + \mathbf{X}^{\mathbf{f}}\mathbf{w}^* + \sqrt{N-1}(\mathbf{X}^{\mathbf{f}}\nabla^{\mathbf{2}}\mathcal{J})_{\mathbf{i}} \tag{4}$$

and

$$\nabla^{\mathbf{2}}\mathcal{J} = (N-1)\mathbf{I_N} + \widetilde{\mathbf{H}}^\top\widetilde{\mathbf{H}} \tag{5}$$

In practice, the anomaly matrix from the analysis $\mathbf{X^a}$ is obtained by the following formula:

$$\mathbf{X^a} = \mathbf{X^f}\mathbf{T} \tag{6}$$

with $\mathbf{T} = (\mathbf{I} + \mathbf{S}\mathbf{S}^\top)^{-1/2} - \mathbf{I}$ and $\mathbf{S} = \frac{1}{\sqrt{N-1}}\mathbf{R}^{-1/2}\mathbf{H}\mathbf{X}^{\mathbf{f}}$

2.2 Reformulation and resolution of ETKF with kernels

Let the previous ETKF problem be embedded in a RKHS (Reproducing Kernel Hilbert Space):

$$(2) \Leftrightarrow \underset{\mathbf{w}\in\mathbb{R}^N}{\arg\min}\,\mathcal{J}(\mathbf{w}) = \frac{N-1}{2}\kappa(\mathbf{w},\mathbf{w}) + \frac{1}{2}\sum_{i=1}^{p}(\kappa(\widetilde{\mathbf{h}_\mathbf{i}},\mathbf{w}) - \widetilde{d}_i)^2 \tag{7}$$

with κ the linear kernel defined by: $\kappa(\mathbf{x},\mathbf{y}) = \mathbf{x}^\top\mathbf{y}$, $\forall\ (\mathbf{x},\mathbf{y}) \in \mathbb{R}^N \times \mathbb{R}^N$.

Considering the RKHS $\mathcal{H}_\kappa$ with reproducing kernel κ, where $\mathcal{H}_\kappa$ is a functional space, (7) is equivalent to:

$$\underset{f\in\mathcal{H}_\kappa}{\arg\min}\,\widetilde{\mathcal{J}}(f) = \frac{N-1}{2}||f||_{\mathcal{H}_\kappa}^2 + \frac{1}{2}\sum_{i=1}^{p}(f(\widetilde{\mathbf{h}_\mathbf{i}}) - \widetilde{d}_i)^2 \tag{8}$$

with $f \in \mathcal{H}_\kappa$ such as: $f : \begin{cases} \mathbb{R}^p \to \mathbb{R} \\ \mathbf{x} \quad \mapsto \kappa(\mathbf{x},\mathbf{w}) \end{cases}$

We thus have extended the previous problem, since we may use any kernel, not only the linear one.

ICCS Camera Ready Version 2023
To cite this paper please use the final published version:
DOI: 10.1007/978-3-031-36027-5_35

We now can apply the representer theorem which leads to an optimisation problem in finite dimension, given by the amount of data $\{(\mathbf{x_j})_{1\leq j\leq n}; (\widetilde{\mathbf{h}}_\mathbf{l})_{1\leq l\leq p}\}$. The equation (8) can then be rewritten:

$$\underset{\alpha\in\mathbb{R}^{p+n}}{\arg\min}\, \widetilde{\widetilde{\mathcal{J}}}(\alpha) = \frac{N-1}{2}\alpha^\top \mathbf{K}\alpha + \frac{1}{2}\|\widetilde{\mathbf{d}} - \mathbf{\Pi_H}\mathbf{K}\alpha\|_2^2 \tag{9}$$

with:

- $\mathbf{\Pi_H} = \begin{bmatrix} \mathbf{0_{nn}} & \mathbf{0_{np}} \\ \mathbf{0_{pn}} & \mathbf{I_p} \end{bmatrix} \in \mathbb{R}^{(n+p)\times(n+p)}$ the projection matrix on the observation space
- $\mathbf{K} = \begin{bmatrix} \mathbf{K_X} & \mathbf{K_{XH}} \\ \mathbf{K_{XH}}^\top & \mathbf{K_H} \end{bmatrix} \in \mathbb{R}^{(n+p)\times(n+p)}$ with
  - $\mathbf{K_X} = (\kappa(\mathbf{a_i^f}, \mathbf{a_j^f}))_{1\leq i,j\leq n} \in \mathbb{R}^{n\times n}$, the kernel applied to state variables
  - $\mathbf{K_{HX}} = (\kappa(\mathbf{a_i^f}, \widetilde{\mathbf{h}}_\mathbf{j}))_{1\leq i\leq n, 1\leq j\leq p} \in \mathbb{R}^{n\times p}$, the crossed kernel application
  - $\mathbf{K_H} = (\kappa(\widetilde{\mathbf{h}}_\mathbf{i}, \widetilde{\mathbf{h}}_\mathbf{j}))_{1\leq i,j\leq p} \in \mathbb{R}^{p\times p}$, the kernel applied to observations

The solution α^* of (9) is then determined with the first order optimality condition:

$$\alpha^* = [(N-1)\mathbf{I_{n+p}} + \mathbf{\Pi_H}\mathbf{K}]^{-1} \begin{bmatrix} \mathbf{0_{n1}} \\ \widetilde{\mathbf{d}} \end{bmatrix} \tag{10}$$

which can be simplified as:

$$\begin{cases} \alpha^*_\mathbf{X} = & \mathbf{0_{n1}} \\ \alpha^*_\mathbf{H} = & [(N-1)\mathbf{I_p} + \mathbf{K_H}]^{-1}\widetilde{\mathbf{d}} \end{cases} \tag{11}$$

with $\alpha^* = \begin{bmatrix} \alpha^*_\mathbf{X} \\ \alpha^*_\mathbf{H} \end{bmatrix} \in \mathbb{R}^{p+n}$.

Thus, the mean of the ensemble after the analysis will be:

$$\bar{\mathbf{x}}^\mathbf{a} = \bar{\mathbf{x}}^\mathbf{f} + \mathbf{K_{XH}}\alpha^*_\mathbf{H} \tag{12}$$

$$\Leftrightarrow \bar{\mathbf{x}}^\mathbf{a} = \bar{\mathbf{x}}^\mathbf{f} + \mathbf{K_{XH}}[(N-1)\mathbf{I_p} + \mathbf{K_H}]^{-1}\widetilde{\mathbf{d}} \tag{13}$$

It requires to solve a linear system of a symmetric positive definite (SPD) matrix.

Ensemble's reconstruction: Now that we have the solution α^*, we must integrate it into the construction of the ensemble resulting from the analysis. The idea is to extend the ensemble to construct by considering the set of variables to be determined not only as the set of observed and unobserved variables $\mathbf{E^a}$ but also the set of transformed observed variables $\mathbf{HE^a}$, as it has already been done in the determination of α^*.

ICCS Camera Ready Version 2023
To cite this paper please use the final published version:
DOI: 10.1007/978-3-031-36027-5_35

The principle of this generation is based on the deterministic version of the Ensemble Kalman Filter (EnKF) algorithm [17]. However, following the strategy formalized in [17], the state vector is extended to include both observed and unobserved variables. Formally, it reads:

$$\begin{bmatrix} \mathbf{E^a} \\ \mathbf{HE^a} \end{bmatrix} = \begin{bmatrix} \bar{\mathbf{x}}^\mathbf{f} \\ \mathbf{H}\bar{\mathbf{x}}^\mathbf{f} \end{bmatrix} + \begin{bmatrix} \mathbf{X^f} \\ \mathbf{HX^f} \end{bmatrix} \mathbf{w} + \sqrt{N-1}\mathbf{P^{a}}^{1/2} \tag{14}$$

with $\mathbf{P^a} = \begin{bmatrix} \mathbf{P^a_X} & \mathbf{P^a_{XH}} \\ \mathbf{P^a_{XH}}^\top & \mathbf{P^a_H} \end{bmatrix} \in \mathbb{R}^{(n+p)\times(n+p)}$ the analysis error covariance matrix.

However, in order to update the ensemble $\mathbf{E^a}$, the block $\mathbf{P^a_X}$ of $\mathbf{P^a}$ is sufficient. Setting $\mathbf{P^a_X} = \mathbf{U\Sigma V}^\top$ the SVD of $\mathbf{P^a_X}$, we truncate $\mathbf{\Sigma}$ to its rank r_Σ ($\widetilde{\mathbf{\Sigma}}$) and the columns of $\mathbf{U}$ are also truncated to r_Σ ($\widetilde{\mathbf{U}}$) to compute the square root of $\mathbf{P^a_X}$. Using (13), this can be written member by member as follows:

$$\forall i \in \{1, ..., N\}, \quad \mathbf{x_i^a} = \bar{\mathbf{x}}^\mathbf{f} + \mathbf{K_{XH}}[(N-1)\mathbf{I_p} + \mathbf{K_H}]^{-1}\widetilde{\mathbf{d}} + [\widetilde{\mathbf{U}}\widetilde{\mathbf{\Sigma}}^{1/2}\mathbf{W}]_i \tag{15}$$

with $\mathbf{W} \in \mathbb{R}^{r_\Sigma \times N}$ a rotation matrix for column augmentation as implemented by [16] and detailed in **Algorithm 3**.

However, we still have to determine the expression of $\mathbf{P^a_X}$ in order to perform the SVD.
From the perspective of random variables, we can write $\alpha \sim \mathcal{N}(\mu_\alpha, \mathbf{P}^\alpha)$ and we can interpret (12) as:

$$\mathbf{x^a} = \bar{\mathbf{x}}^\mathbf{f} + \mathbf{\Pi_X K}\alpha \tag{16}$$

where $\mathbf{\Pi_X} = \begin{bmatrix} \mathbf{I_n} & \mathbf{0_{np}} \end{bmatrix}$ and $\mathbf{x^a} \sim (\mu_\mathbf{a}, \mathbf{P^a_X})$. Thus,

$$\mathbf{P^a_X} = Cov(\mathbf{x_i^a}, \mathbf{x_j^a}) = \mathbf{\Pi_X K P}^\alpha \mathbf{K \Pi_X} \tag{17}$$

where $(\mathbf{x_i^a}, \mathbf{x_j^a})_{1\leq(i,j)\leq n}$ are randoms draws of $\mathbf{x^a}$.

According to [15], $\mathbf{P}^\alpha$ can be approximated by:

$$\mathbf{P}^\alpha \approx [\nabla^\mathbf{2}\widetilde{\widetilde{\mathcal{J}}}]^{-1} \tag{18}$$

and

$$\nabla^\mathbf{2}\widetilde{\widetilde{\mathcal{J}}} = [(N-1)\mathbf{K} + \mathbf{K\Pi_H\Pi_H K}] \tag{19}$$

Case where K is not invertible: Since $\mathbf{K}$ may be singular, we thus calculate an approximation of $\nabla^\mathbf{2}\widetilde{\widetilde{\mathcal{J}}}$ from de generalized inverse by truncating the SVD of the matrix at rank of $\mathbf{K}$:
We set $\nabla^\mathbf{2}\widetilde{\widetilde{\mathcal{J}}} = \mathbf{V}_\mathcal{J}\mathbf{\Sigma}_\mathcal{J}\mathbf{U}_\mathcal{J}^\top = \widetilde{\mathbf{V}_\mathcal{J}}\widetilde{\mathbf{\Sigma}_\mathcal{J}}\widetilde{\mathbf{U}_\mathcal{J}}^\top$ with $\widetilde{\mathbf{V}_\mathcal{J}}$, $\widetilde{\mathbf{\Sigma}_\mathcal{J}}$ and $\widetilde{\mathbf{U}_\mathcal{J}}^\top$ the respective matrix of $\mathbf{V}_\mathcal{J}, \mathbf{\Sigma}_\mathcal{J}, \mathbf{U}_\mathcal{J}{}^\top$ truncated at the rank of $\mathbf{K}$. Thus,

$$\mathbf{P^a_X} = \mathbf{\Pi_X K}\widetilde{\mathbf{V}_\mathcal{J}}\widetilde{\mathbf{\Sigma}_\mathcal{J}}\widetilde{\mathbf{U}_\mathcal{J}}^\top\mathbf{K\Pi_X} \tag{20}$$

ICCS Camera Ready Version 2023
To cite this paper please use the final published version:
DOI: 10.1007/978-3-031-36027-5_35

Depending on the chosen kernel, the rank of $\mathbf{K}$ can be less than N. We then have to augment the columns of $\mathbf{P_X^a}^{1/2}$ in order to keep the same number of ensemble members. Appendix A of [16] gives an algorithm to augment an ensemble covariance matrix $\mathbf{P_X^a}$ while keeping the same empirical covariance $\left(\widetilde{\mathbf{P_X^a}}^{1/2}\right)^T\left(\widetilde{\mathbf{P_X^a}}^{1/2}\right)$ and $\widetilde{\mathbf{P_X^a}}^{1/2}$ centered. We include this algorithm in the ensemble reconstruction.

The case where K is invertible is provided in Annex A, which gives an analytical expression for $\mathbf{P_X^a}$.

The method presented above is summarized in the form of **Algorithms 1**, **2** and **3**.

Algorithm 1 ETKF kernel analysis

$\widetilde{\mathbf{H}} \leftarrow \mathbf{R}^{-1/2}\mathbf{H}\mathbf{X^f}$
$\widetilde{\mathbf{d}} \leftarrow \mathbf{R}^{-1/2}(\mathbf{y} - \mathbf{H}\bar{\mathbf{x}}^\mathbf{f})$
Compute $\mathbf{K}$ ▷ depends on the chosen kernel
$\alpha^*_\mathbf{H} = [(N-1)\mathbf{I_p} + \mathbf{K_H}]^{-1}\widetilde{\mathbf{d}}$ ▷ Solve a linear system of a SPD matrix
$\bar{\mathbf{x}}^\mathbf{a} = \bar{\mathbf{x}}^\mathbf{f} + \mathbf{K_{XH}}^\top \alpha^*_\mathbf{H}$
Compute $\mathbf{\Sigma}$, $\mathbf{U}$ the singular values and vectors of $\mathbf{P_X^a}$ ▷ refer to **Algorithm 2**
Truncate $\mathbf{\Sigma}$ to its rank r_Σ and compute its square root: $\widetilde{\mathbf{\Sigma}}^{1/2}$
$\mathbf{P_X^a}^{1/2} \leftarrow \widetilde{\mathbf{U}}\widetilde{\mathbf{\Sigma}}^{1/2}$ ▷ with $\widetilde{\mathbf{U}}$, the first r_Σ columns of $\mathbf{U}$
for i = 1... N-r_Σ **do**
  rotate $\mathbf{P_X^{a^{1/2}}}$ following the rotation step of **Algorithm 3**
end for
$\mathbf{E} = \bar{\mathbf{x}}^\mathbf{a} + \sqrt{N-1}\mathbf{P_X^a}^{1/2}$

Algorithm 2 Computation of $\mathbf{P_X^a}$

if K is not invertible **then**
  Compute $\nabla^\mathbf{2}\widetilde{\mathcal{J}} \leftarrow [(N-1)\mathbf{K} + \mathbf{K\Pi_H\Pi_H K}]$
  Compute the SVD of $\nabla^\mathbf{2}\widetilde{\mathcal{J}} = \mathbf{U}_\mathcal{J}\mathbf{\Sigma}_\mathcal{J}\mathbf{V}_\mathcal{J}^\top$
  Compute $\widetilde{\mathbf{U}_\mathcal{J}}$, $\widetilde{\mathbf{\Sigma}_\mathcal{J}}$ and $\widetilde{\mathbf{V}_\mathcal{J}}^\top$ the respective matrix of $\mathbf{U}_\mathcal{J}, \mathbf{\Sigma}_\mathcal{J}, \mathbf{V}_\mathcal{J}{}^\top$ truncated at the rank of $\mathbf{K}$
  $\mathbf{\Sigma} \leftarrow \mathbf{\Sigma}_\mathcal{J}^{-\mathbf{1}}$
  Compute $\mathbf{U} \leftarrow \mathbf{\Pi_X K}\widetilde{\mathbf{U}_\mathcal{J}}$ ▷ $\mathbf{P_X^{a^{1/2}}} = \mathbf{U\Sigma^{1/2}}$
else
  Compute $\mathbf{P_X^a} \leftarrow \mathbf{K_X} - \mathbf{K_{HX}U_H}diag(\frac{1}{(N-1)+\lambda_i})\mathbf{U_H}^\top\mathbf{K_{HX}}^\top$ ▷ with $[\lambda_i]_{1\leq i\leq n}$ the eigenvalues of $\mathbf{K_H}$
  Compute the SVD of $\mathbf{P_X^a} = \mathbf{U\Sigma V}^\top$
end if

ICCS Camera Ready Version 2023
To cite this paper please use the final published version:
DOI: 10.1007/978-3-031-36027-5_35

Algorithm 3 Rotation step of $\mathbf{P_X^{a^{1/2}}}$, directly derived from Annex A of [16]

Require: $1 \leq i \leq N - r_\Sigma$

$\epsilon \leftarrow 1.0$

Compute $q \leftarrow r_\Sigma + i$

Compute $\theta \leftarrow \frac{\sqrt{q}}{\sqrt{q}-\epsilon}$

Compute $\mathbf{Q}_\epsilon \leftarrow \frac{-\theta}{q} \times \begin{bmatrix} \frac{\epsilon}{\sqrt{q}} & \cdots & \cdots & \cdots & \cdots & \frac{\epsilon}{\sqrt{q}} \\ \vdots & 1-\frac{\theta}{q} & \frac{-\theta}{q} & \cdots & \cdots & \frac{-\theta}{q} \\ \vdots & \frac{-\theta}{q} & 1-\frac{\theta}{q} & \frac{-\theta}{q} & \cdots & \frac{-\theta}{q} \\ \vdots & \vdots & \ddots & \ddots & \ddots & \vdots \\ \vdots & \vdots & \ddots & \ddots & 1-\frac{\theta}{q} & \frac{-\theta}{q} \\ \frac{\epsilon}{\sqrt{q}} & \frac{-\theta}{q} & \cdots & \cdots & \frac{-\theta}{q} & 1-\frac{\theta}{q} \end{bmatrix} \in \mathbb{R}^{q \times q}$

$\mathbf{W} \leftarrow \left[\mathbf{0_n}\ \mathbf{P_X^{a^{1/2}}}\right] \in \mathbb{R}^{n \times q}$

Compute $\mathbf{P_X^{a^{1/2}}} \leftarrow \mathbf{W}\mathbf{Q}_\epsilon$

3 Numerical experiments

In the following, we perform numerical experiments in order to compare the Root Mean Square Errors (RMSE) of the ETKF and the proposed Kernel ETKF.

3.1 Experimental setup

These experiments are performed using the Lorenz 63 model, which is a simplified chaotic and nonlinear model for atmospheric convection, widely used in data assimilation to benchmark. It is defined by the following differential equations:

$$\begin{cases} \frac{dx}{dt} = & \sigma(y-x) \\ \frac{dy}{dt} = & \rho x - y - xz \\ \frac{dz}{dt} = & xy - \beta z. \end{cases} \tag{21}$$

These equations are integrated through a fourth-order Runge-Kutta scheme with a time-step of $\delta t = 0.01$, $\sigma = 10$, $\rho = 28$, $\beta = 8/3$, as set in [19] and [18]. The initial condition is distributed according to a Gaussian distribution of mean $[1.509, -1.531, 25.46]$ and a covariance matrix set to $\mathbf{C} = 2 * \mathbf{I_3}$.

A graphic representation of the Lorenz 63 model is given in Figure 1 (a). For all experiments, we computed the average RMSE over 10 different seeds (generating observations, initial state...).

In a first set of experiments, we compare the initial ETKF and Kernel ETKF applied to the linear kernel:

$$\forall (\mathbf{x}, \mathbf{y}) \in \mathbb{R}^N \times \mathbb{R}^N, \quad \kappa(\mathbf{x}, \mathbf{y}) = \mathbf{x}^\top \mathbf{y} \tag{22}$$

ICCS Camera Ready Version 2023
To cite this paper please use the final published version:
DOI: 10.1007/978-3-031-36027-5_35

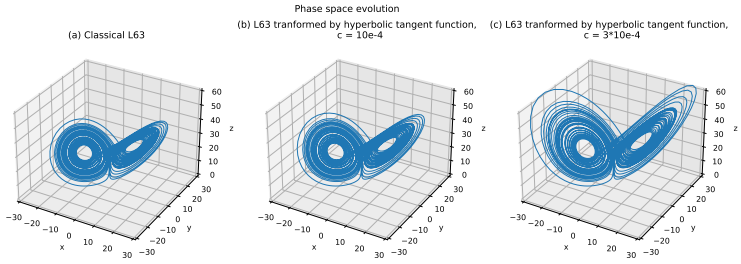

Fig. 1. Phase space evolution of the Lorenz 63 model: (a) classical L63; (b) L63 tranformed by hyperbolic tangent fonction (25) with $c = 10^{-4}$; (c) L63 tranformed by hyperbolic tangent fonction (25) with $c = 3 \times 10^{-4}$ to accentuate the visual effect

.

The observations are generated every $\delta to = 0.02$, as set in [19], with $\mathbf{R} = 2 * \mathbf{I_3}$ and we set $\mathbf{H} = \begin{bmatrix} 1 & 0 & 0 \\ 0 & 1 & 0 \end{bmatrix}$, observing only the two first variables. A burn-in period of $5 \times 10^3 \times \delta to$ is enforced, as set in [19]. For these experiments, we use 5×10^5 observations vectors which determines the number of cycles. We compare different inflation factors: $infl \in \{1.0, 1.04, 1.1\}$. For each inflation factor, the evaluated ensemble sizes were $N \in \{3, 6, 9, 10, 12, 15\}$.

In a second set of experiments, we compare the performances of the initial ETKF and the Kernel ETKF applied to a non linear kernel: the hyperbolic tangent one. The hyperbolic tangent kernel is defined as in [20] by:

$$\forall (\mathbf{x}, \mathbf{y}) \in \mathbb{D}_c^N \times \mathbb{D}_c^N, \quad \kappa(\mathbf{x}, \mathbf{y}) = \phi(\mathbf{x})^\top \phi(\mathbf{y}) \tag{23}$$

where $\mathbb{D}_c^N$ is the Poincaré ball:

$$\mathbb{D}_c^N = \{z \in \mathbb{R}^N : c||z|| < 1\} \tag{24}$$

and

$$\forall c > 0, \ \ \forall \mathbf{z} \in \mathbb{D}_c^N, \quad \phi(\mathbf{z}) = tanh^{-1}(\sqrt{c}||\mathbf{z}||)\frac{\mathbf{z}}{\sqrt{c}||\mathbf{z}||} \tag{25}$$

A representation of the Lorenz 63 transformation induced by the hyperbolic tangent kernel with $c = 10^{-4}$ and $c = 3 \times 10^{-4}$ are given in Figure 1 (b) and (c) respectively. One can notice that L63 is sensitive to small variations of the c parameter. Quantile-quantile plots are given in Figure 2 in order to compare the initial distribution of each variable of the L63 and the distribution after applying the hyperbolic tangent function with $c = 10^{-4}$ and $c = 3 \times 10^{-4}$ to the normal distribution. This last case is presented only to exacerbate the visual effect of the transformation induced by the kernel but will not be used for the Kernel ETKF experiments, because the transformation is too important to allow a regular convergence of the method. The QQ-plots confirm that the L63 variables have shorter tails than the Gaussian distribution but the hyperbolic tangent stretches

ICCS Camera Ready Version 2023
To cite this paper please use the final published version:
DOI: 10.1007/978-3-031-36027-5_35

the tails of the x and y variables closer to the Gaussian. The third variable z still shows short tails after the transformation, probably because the two L63 attractors share the same coordinate z=0. This can probably be further improved by fine tuning a different value of the c parameter for the z variable.

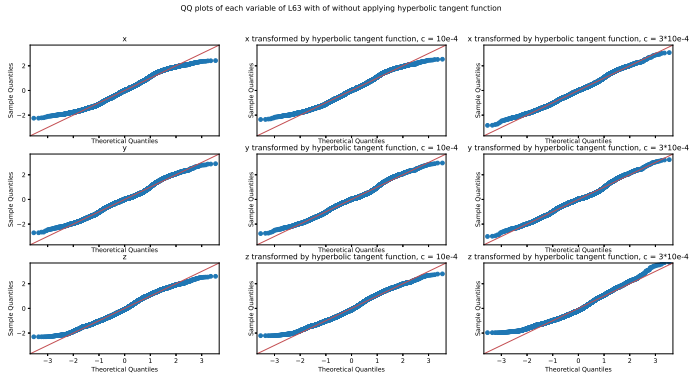

Fig. 2. QQ plots of each variable of the L63 relative to the normal distribution, Left: classical L63; Middle: L63 tranformed by hyperbolic tangent fonction (25) with $c = 10^{-4}$; Right: L63 tranformed by hyperbolic tangent fonction (25) with $c = 3 \times 10^{-4}$ to accentuate the visual effect

.

First, we set $\mathbf{H} = \mathbf{I_3}$ and we change the time between the generation of observations to $\delta to = 0.50$ to reinforce the nonlinearities. We use 2×10^4 observation vectors and a burn-in period of $2 \times 10^2 \times \delta to$.

We then compute a last set the experiments with $\mathbf{H} = \begin{bmatrix} 1 & 0 & 0 \\ 0 & 1 & 0 \end{bmatrix}$, observing only the first two variables. For this set, we set $\delta to = 0.25$ and we use 5×10^4 observation vectors. A burn-in period of $5 \times 10^2 \times \delta to$ is enforced.

For these experiments, we computed the average RMSE over 10 different seeds for the two methods, using five ensembles sizes: $N = \{3, 6, 10, 12, 15\}$ for which different inflation factors have been evaluated: $infl \in \{1.0, 1.04, 1.1\}$.

For all the experiments presented here, we used the python package DAPPER [18], which allows benchmarking of performances of data assimilation methods. Several methods of data assimilation, both ensemble-based and variational, are already implemented in the package. We have also implemented our Kernel ETKF method.

3.2 Discussion

Comparison of the classical ETKF and the Kernel ETKF applied to the linear kernel: In Figure 3, we represent the average RMSE of both meth-

ICCS Camera Ready Version 2023
To cite this paper please use the final published version:
DOI: 10.1007/978-3-031-36027-5_35

ods with different ensemble sizes and different inflation factors when only two variables observed. We expect similar performances, as the two formulations are theoretically equivalent for the linear kernel. Any differences would be due to the method of ensemble reconstruction.

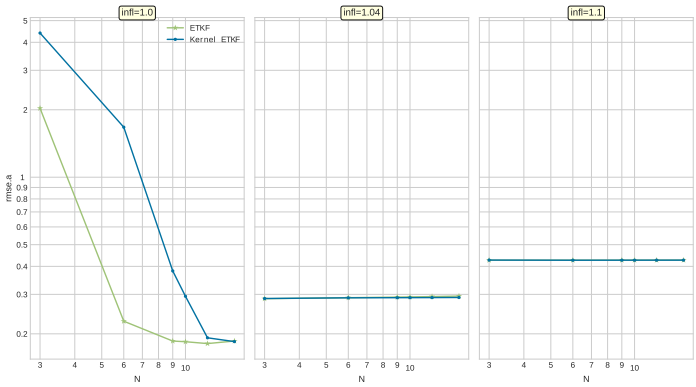

Fig. 3. Average RMSE obtained by ETKF (in green) and linear Kernel ETKF (in blue) assimilation methods when applied to the Lorenz 63 model and observing only the first two variables. The average is computed upon 10 different seeds generating observations, initial state... On each subfigure, a different inflation factor is applied to each method: Left: no inflation (infl = 1.0), Middle: infl = 1.04, Right: infl = 1.1. In each subfigure, different ensemble sizes N were tested, in each case $N \in \{3, 6, 9, 10, 12, 15\}$.

When $infl \neq 1.0$, in Figure 3, the results of the two methods are similar, as expected. However, the Kernel ETKF seems more sensitive to the absence of inflation than the classical ETKF. This could be due to the implementation of ensemble reconstruction for the Kernel ETKF method, and in particular to sampling issues.

We obtain similar results when all variables of the L63 are observed: the Kernel ETKF has equivalent results with the classical ETKF, except without inflation where it shows a slower convergence. The presented results show the equivalent performance (when using some inflation) of the classical ETKF and the linear kernel-based approach proposed here as expected.

Experiments with non linearity reinforcement and non linear kernels: In this perspective, we have carried out another set of experiments, this time increasing the time between the generation of observations to reinforce the non-linearities in the data assimilation experiments. We tested the performance of a non linear kernel. We present here the results for the hyperbolic tangent kernel with $c = 10^{-4}$ which presented the best performances among the tested kernels. In Figures 4 and 5, we give the average RMSE of both methods with different

ICCS Camera Ready Version 2023
To cite this paper please use the final published version:
DOI: 10.1007/978-3-031-36027-5_35

ensemble sizes and different inflation factors when all variables are observed in Figure 4 and only two variables observed in Figure 5.

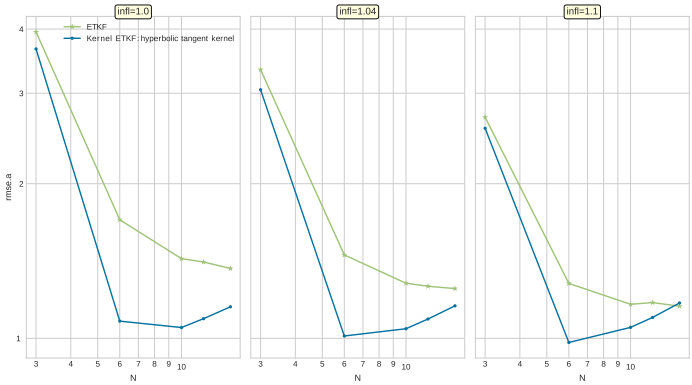

Fig. 4. Average RMSE obtained by ETKF (in green) and Kernel ETKF applied to hyperbolic tangent kernel with $c = 10^{-4}$ (in blue) when applied to the Lorenz 63 model and observing all variables. The average is computed upon 10 different seeds generating observations, initial state... Left: $infl = 1.0$. Middle: $infl = 1.04$. Right: $infl = 1.1$. For each subfigure, different ensemble sizes are tested: $N \in \{3, 6, 10, 12, 15\}$.

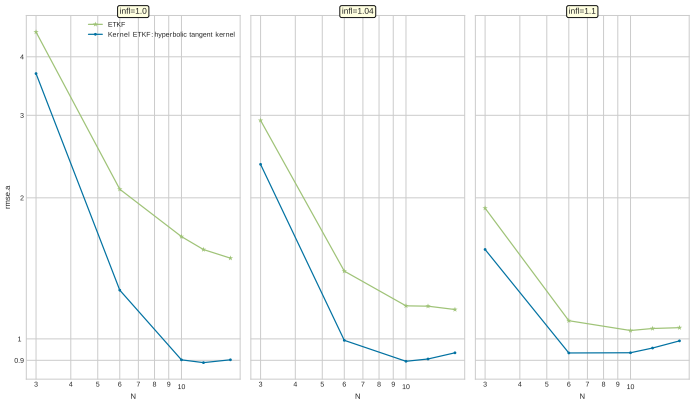

Fig. 5. Average RMSE obtained by ETKF (in green) and Kernel ETKF applied to hyperbolic tangent kernel with $c = 10^{-4}$ (in blue) when applied to the Lorenz 63 model and observing the first two variables. The average is computed upon 10 different seeds generating observations, initial state... Left: $infl = 1.0$. Middle: $infl = 1.04$. Right: $infl = 1.1$. In each one, different ensemble sizes are tested: $N \in \{3, 6, 10, 12, 15\}$.

ICCS Camera Ready Version 2023
To cite this paper please use the final published version:
DOI: 10.1007/978-3-031-36027-5_35

In both cases, the hyperbolic tangent Kernel ETKF has a clear advantage over the classical ETKF, especially for small sets, which seems particularly promising for large problems, where set size is a key issue. However, we can note an increase in RMSE for large ensemble sizes for the hyperbolic tangent Kernel ETKF. This increase was already observed in [21], and seems intrinsically linked to the ETKF. The hyperbolic tangent Kernel ETKF being more efficient for small ensemble sizes, it is logical that the above mentioned problem occurs earlier. This problem of RMSE increase can be corrected by introducing a rotation after the analysis, as proposed in [22].

In Figure 6, we take a closer look at the similarities between the ensemble spread (experimental measure of forecast error) and the RMSE (exact measure of forecast error) for each variable of the system in the case where $N = 10$, $infl = 1.04$ and the two first variables are observed (same as in Figure 5). We note that the RMSE of the classical ETKF is globally further from the spread than the one of the Kernel ETKF, which explains in this case the overall difference in RMSE between the two methods and the fact that the Kernel ETKF gives an overall better result than the classical ETKF. Some statistics for this experiment are given in **Table 1**. The advantage of the Kernel ETKF over the classical ETKF is highlighted: the RMSE of each model variable is lower for the Kernel ETKF than for the classical ETKF.

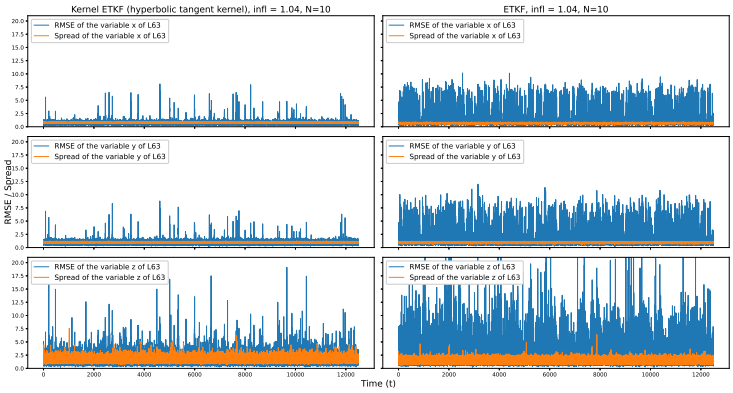

Fig. 6. Ensemble spread (in orange) and RMSE (in blue) obtained by hyperbolic tangent Kernel ETKF (left panel) and classical ETKF (right panel) assimilation methods when applied to the Lorenz 63 model and observing the first two variables variables in the case where $N = 10$, $infl = 1.04$. The ensemble spread and RMSE are displayed for each three variables of the L63 model individually.

ICCS Camera Ready Version 2023
To cite this paper please use the final published version:
DOI: 10.1007/978-3-031-36027-5_35

	ETKF		Kernel ETKF	
L63 variable	RMSE	Spread	RMSE	Spread
x	1.1 ± 1.0	0.68 ± 0.062	**0.69 ± 0.28**	0.75 ± 0.057
y	1.4 ± 1.1	0.93 ± 0.082	**0.93 ± 0.32**	1.0 ± 0.069
z	2.2 ± 1.7	1.4 ± 0.37	**1.5 ± 0.82**	1.7 ± 0.43

Table 1. RMSE and Spread of each variables for the hyperbolic tangent Kernel ETKF and the classical ETKF when applied to the Lorenz 63 model and observing the first two variables variables in the case where $N = 10$, $infl = 1.04$.

4 Conclusion and Perspectives

In this paper, we have proposed a generalisation of the ETKF problem by introducing kernels into its formulation. We also proposed a reconstruction of the set from the solution of the optimisation problem induced by the formulation. An explicit algorithm for this method is given. In a second part, we compared the performance of the proposed method with the linear kernel and the hyperbolic tangent kernel with that of the ETKF in the Lorenz 63 framework. We obtained similar performances for the linear kernel which was theoretically expected. We also could envisage the interest of using other kernels with the results of the hyperbolic tangent kernel when the model presents important nonlinearities, which is encouraging for the continuation of our research: the interest of the kernel methods will intervene when we will address systems where the use of non-linear kernels (such as the Gaussian or hyperbolic tangent kernels) will be more appropriate for the given data. Moreover, the good results obtained with the hyperbolic tangent kernel are particularly interesting in the case of small ensembles, since the size of the ensemble is a key issue when dealing with high dimensional problems.

We are currently considering the integration of localisation into our method: for localisation by Schur product, we consider as localisation matrix an exponential kernel matrix with respect to the distances between the variables and the observations. The Schur product with our kernel matrix on the data retains the kernel characteristic and we can then apply the resolution on this new matrix. For domain-based localisation, the local analysis as proposed in the LETKF of [14], implemented in DAPPER [18], is easily modified to be applied to our method, which would have advantages in terms of resolution cost and parallelisation of the method.

References

1. Buehner, M., McTaggart-Cowan, R., Heilliette, S.: An Ensemble Kalman Filter for Numerical Weather Prediction Based on Variational Data Assimilation: VarEnKF. In: Monthly Weather Review 145.2 (2017), p. 617-635. https://doi.org/10.1175/MWR-D-16-0106.1

ICCS Camera Ready Version 2023
To cite this paper please use the final published version:
DOI: 10.1007/978-3-031-36027-5_35

2. Carrassi, A, Bocquet, M, Bertino, L, Evensen, G.: Data assimilation in the geosciences: An overview of methods, issues, and perspectives. In: WIREs Clim Change (2018). https://doi.org/https://doi.org/10.1002/wcc.535
3. Tsuyuki, T., Miyoshi, T.: Recent Progress of Data Assimilation Methods in Meteorology. In: Journal of the Meteorological Society of Japan. Ser. II 85B (2007), p. 331-361. https://doi.org/10.2151/jmsj.85B.331
4. Sakov, P., Counillon, F., Bertino, L., Lisæter, K. A., Oke, P. R., and Korablev, A.: TOPAZ4: an ocean-sea ice data assimilation system for the North Atlantic and Arctic. In: Ocean Sci. 8 (2012), p. 633–656. https://doi.org/10.5194/os-8-633-2012
5. Barth, A., Canter, M., van Schaeybroeck, B., Vannitsem, S., Massonnet, F., Zunz, V., Mathiot, P., Alvera-Azcaráte, A., Beckers, J.-M.: Assimilation of sea surface temperature, ice concentration and ice drift in a model of the Southern Ocean. In: Ocean Modelling 93 (2015), p. 22– 39.
6. Lei, J., Bickel, P., Snyder, C.: Comparison of Ensemble Kalman Filters under Non-Gaussianity. In: Monthly Weather Review 138.4 (2010), p. 1293-1306. https://doi.org/10.1175/2009MWR3133.1
7. Bertino, L., Evensen, G., Wackernagel, H.: Sequential Data Assimilation Techniques in Oceanography. In: International Statistical Review 71.2 (2003), p 223–241. https://doi.org/https://doi.org/10.1111/j.1751-5823.2003.tb00194.x
8. Simon, E., Bertino, L.: Application of the Gaussian anamorphosis to assimilation in a 3-D coupled physical-ecosystem model of the North Atlantic with the EnKF: A twin experiment. Ocean Science (OS) (march 2009). https://doi.org/10.5194/os-5-495-2009
9. Grooms, I.: A comparison of nonlinear extensions to the ensemble Kalman filter". In: Computational Geosciences 26.3 (2022), p. 633-650. https://doi.org/10.1007/s10596-022-10141-x
10. Luo, X.: Ensemble-based kernel learning for a class of data assimilation problems with imperfect forward simulators. In: PLOS ONE 14.7 (july 2019), p. 1-40. https://doi.org/10.1371/journal.pone.0219247
11. D.S. Broomhead, D. Lowe: Radial basis functions, multivariable functional interpolation and adaptive networks. In: Royal Signals and Radar Establishment Malvern (1988).
12. G.A. Gottwald, S. Reich: Supervised learning from noisy observations: Combining machine-learning techniques with data assimilation. In: Physica D: Nonlinear Phenomena (2021). https://doi.org/10.1016/j.physd.2021.132911
13. B. Hug, E. Mémin, G. Tissot: Ensemble forecast in reproducing kernel Hilbert space family: dynamical systems in Wonderland. arXiv:2207.14653 (2022). https://doi.org/10.48550/arxiv.2207.14653
14. Hunt, B. R., Kostelich, E. J., Szunyogh, I.: Efficient data assimilation for spatio-temporal chaos: A local ensemble transform Kalman filter. In: Physica D: Nonlinear Phenomena 230.1 (2007). Data Assimilation, p. 112-126. https://doi.org/10.1016/j.physd.2006.11.008
15. Didier Auroux Homepage, https://math.unice.fr/ auroux/Work/These/html/node40.html. Last accessed 29 jan 2023
16. Farchi, A., Bocquet, M.: On the Efficiency of Covariance Localisation of the Ensemble Kalman Filter Using Augmented Ensembles. In: Frontiers in Applied Mathematics and Statistics 5 (2019). https://doi.org/10.3389/fams.2019.00003
17. Evensen, G.: Data Assimilation: The Ensemble Kalman Filter. 2nd edn. Springer, Verlag Berlin Heidelberg (2009), p.273-274.

ICCS Camera Ready Version 2023
To cite this paper please use the final published version:
DOI: 10.1007/978-3-031-36027-5_35

18. Raanes, P. N., Chen, Y., Grudzien, C., Tondeur, M., Dubois, R. https://github.com/nansencenter/DAPPER. v. 1.2.1. https://doi.org/10.5281/zenodo.2029296
19. Fillion, A., Bocquet, M., Gratton, S.: Quasi-static ensemble variational data assimilation: a theoretical and numerical study with the iterative ensemble Kalman smoother. In: Nonlinear Processes in Geophysics 25 (2018), p.315-334. https://doi.org/0.5194/npg-25-315-2018
20. Fang, P., Harandi, M., Petersson, L.: Kernel Methods in Hyperbolic Spaces. In: Proceedings of the IEEE/CVF International Conference on Computer Vision (ICCV) (Oct. 2021), p. 10665-10674. https://doi.org/10.1109/ICCV48922.2021.01049
21. Sakov, P., Oke, P.R.: A deterministic formulation of the ensemble Kalman filter: an alternative to ensemble square root filters. In: Tellus A (2008), 60: 361-371. https://doi.org/10.1111/j.1600-0870.2007.00299.x
22. Sakov, P., P. R. Oke: Implications of the Form of the Ensemble Transformation in the Ensemble Square Root Filters. In: Mon. Wea. Rev. (2008), 136, 1042–1053, https://doi.org/10.1175/2007MWR2021.1.

A Construction of P^a when K is invertible

We consider the expression of $\mathbf{P^a}$ given by (17):

$$\mathbf{P^a} = \mathbf{K}\mathbf{P}^{\alpha}\mathbf{K}$$

and substitute for $\mathbf{P}^{\alpha}$ its approximation by the hessian (18):

$$\mathbf{P^a} = \mathbf{K}[(N-1)\mathbf{K} + \mathbf{K}\mathbf{\Pi_H}\mathbf{\Pi_H}\mathbf{K}]^{-1}\mathbf{K} \tag{26}$$

Since $\mathbf{K}$ is invertible,

$$\Leftrightarrow \mathbf{P^a} = \frac{1}{N-1}(\mathbf{K}^{-1} + \frac{1}{N-1}\mathbf{\Pi_H}\mathbf{\Pi_H})^{-1} \tag{27}$$

We the apply Woodbury identity:

$$\Leftrightarrow \mathbf{P^a} = \frac{1}{N-1}(\mathbf{K} - \mathbf{K}\mathbf{\Pi_H}((N-1)\mathbf{I_{n+p}} + \mathbf{\Pi_H}\mathbf{K}\mathbf{\Pi_H})^{-1}\mathbf{\Pi_H}\mathbf{K}) \tag{28}$$

$$\Leftrightarrow \mathbf{P^a} = \frac{1}{N-1}(\mathbf{K} - \begin{bmatrix} \mathbf{0_n} & \mathbf{K_{HX}} \\ \mathbf{0_{pn}} & \mathbf{K_H} \end{bmatrix} \begin{bmatrix} (N-1)\mathbf{I_n} & \mathbf{0_{np}} \\ \mathbf{0_{pn}} & (N-1)\mathbf{I_p} + \mathbf{K_H} \end{bmatrix}^{-1} \begin{bmatrix} \mathbf{0_n} & \mathbf{0_{np}} \\ \mathbf{K_H}\mathbf{X}^{\top} & \mathbf{K_H} \end{bmatrix}) \tag{29}$$

Let $\mathbf{K_H}$ decompose as $\mathbf{K_H} = \mathbf{U_H}\mathbf{\Sigma_H}{\mathbf{U_H}}^{\top}$ with $\mathbf{\Sigma_H} = diag([\lambda_i]_{1\leq i\leq p})$ and $[\lambda_i]_{1\leq i\leq p}$ the eigenvalues of $\mathbf{K_H}$. We finally obtain:

$$\mathbf{P^a} = \frac{1}{N-1}\begin{bmatrix} \mathbf{K_X} - \mathbf{K_{HX}}\mathbf{U_H}diag(\frac{1}{(N-1)+\lambda_i}){\mathbf{U_H}}^{\top}{\mathbf{K_{HX}}}^{\top} & \mathbf{K_{HX}} - \mathbf{K_{HX}}\mathbf{U_H}diag(\frac{\lambda_i}{(N-1)+\lambda_i}){\mathbf{U_H}}^{\top} \\ {\mathbf{K_{HX}}}^{\top} - \mathbf{U_H}diag(\frac{\lambda_i}{(N-1)+\lambda_i}){\mathbf{U_H}}^{\top}{\mathbf{K_{HX}}}^{\top} & \mathbf{U_H}diag(\frac{\lambda_i(N-1)}{(N-1)+\lambda_i}){\mathbf{U_H}}^{\top} \end{bmatrix} \tag{30}$$

This gives an explicit expression for $\mathbf{P^a}$ which does not require numerical inversion.

ICCS Camera Ready Version 2023
To cite this paper please use the final published version:
DOI: 10.1007/978-3-031-36027-5_35